JMEPEG (2010) 19:1208–1213
DOI: 10.1007/s11665-010-9595-3

Wear of A380M Aluminum Alloy Under Reciprocating Load

Md. Aminul Islam and Z. Farhat

(Submitted October 17, 2009; in revised form December 15, 2009)

Due to their excellent strength to weight ratio, aluminum alloys are widely used in a variety of automotive components. Their relatively low melting point and low hardness compared to other engineering alloys, however, limits their use in applications where wear resistance is needed. To improve the wear resistance of these alloys, a good understanding of their wear behavior is essential. Dry sliding wear behavior of A380M aluminum alloy was investigated in the load range 6-20 N against steel ball using a reciprocating ball-on-flat configuration and at a frequency range of 4-20 Hz. Micromechanical properties were measured using a nano-indentation system. Scanning electron microscope examination of the wear track and debris revealed that wear within the present load and frequency range was due to abrasion, plastic deformation, and delamination. It was found that the wear rate of A380M aluminum alloy increased with load and decreased with increase in frequency.

Keywords aluminum, automotive, surface engineering, tribology

1. Introduction

Aluminum-silicon alloys are increasingly used (due to their high strength/weight ratio) in automotive engine components, such as pistons, clutch housings, and liners, in which tribological properties of the material are important. For example, in clutch housings, a piston slides into a piston cavity known as "seal surface." The reciprocating friction between the piston and seal surface creates wear damage leading to premature failure.

The wear behavior of aluminum alloys depends on a number of material-related parameters, i.e., size, shape, composition, and distribution of micro constituents, in addition to mechanical properties and service conditions such as load, sliding speed, temperature, and interface condition (Ref 1). Wear mechanism maps developed by Liu et al. (Ref 2) suggest that wear of aluminum alloy occurs by several mechanisms, i.e., oxidation-dominated wear, delamination wear, melt lubrication wear, and seizure. At relatively low sliding speeds and loads, a purely oxidative mechanism controls the process (mild wear). At higher loads, metal-metal contact leads to severe wear when the surface temperature of the contact area exceeds the recrystallization temperature of the material (Ref 3). Subramanian (Ref 4) suggested that the wear rate of Al-Si alloy decreases with increasing sliding speed. He attributed the decreasing trend of wear rate to the reduction in the number and size of the transferred fragments. Jasim and Dwarakadasa (Ref 5) found that the depth of the subsurface damage decreases with increasing sliding speed, indicating that the decrease in wear rate is a consequence of shallower subsurface damage as sliding speed increases. Other researchers concluded that the wear rate initially decreases and then increase (Ref 6) as the sliding speed is steadily increased.

Furthermore, wear transitions in aluminum alloys are common (Ref 7, 8). As load, speed, sliding distance, or temperature varies during wear, operating wear mechanisms may also change leading to wear transitions. It has been found that aluminum alloys exhibit mild to severe wear transition when the surrounding temperature is increased above a critical temperature (Ref 9). On the other hand, Zhang and Alpas (Ref 10) found that at low loads, wear is mild and the wear rate gradually increases with increasing load up to some critical load where transition from mild to severe wear occurs.

Unfortunately, there is only limited work on A380M aluminum alloy under reciprocating loads. In this study, the wear behavior of A380M aluminum alloy is investigated through a series of reciprocating wear tests in an attempt to provide an understanding of wear behavior of A380M as a function of load and frequency.

2. Experimental Details

High-pressure die cast A380M aluminum clutch housing was obtained from Magna Powertrain. Specimens were cut from the seal surface and were prepared for metallographic examinations by grinding using 240, 320, 400, and 600 grit SiC abrasive papers and then polishing using 0.3 and 0.05 μm gama alumina suspension. The composition of A380M aluminum alloy was determined using inductively coupled plasma mass spectrometry, and is summarized in Table 1. The letter 'M' in A380M indicates higher manganese content. High silicon content helps to increase fluidity and improves corrosion resistance (Ref 11-13). Furthermore, the presence of silicon as

Md. Aminul Islam and **Z. Farhat**, Materials Engineering Program, Department of Process Engineering and Applied Science, Dalhousie University, Halifax, NS B3J 2X4, Canada. Contact e-mails: md708166@dal.ca and zoheir.farhat@dal.ca.

Table 1 Composition of A380M aluminum alloy

Composition, wt.%					
Si	Cu	Fe	Mn	Mg	Zn
8.35	3.06	0.87	0.31	0.06	2.15

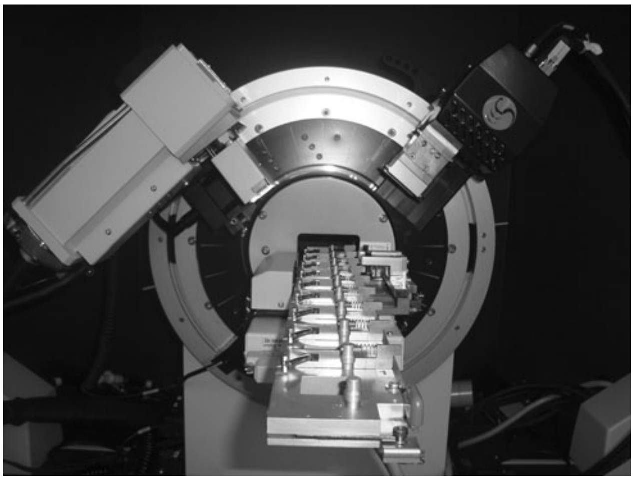

Fig. 1 Bruker D8 XRD system

an alloying element in these alloys improves wear resistance significantly. However, there is no universal trend in wear behavior of Al-Si alloys with respect to silicon content (Ref 14). That is, increasing the Si content in the alloy does not always increase the wear resistance. The presence of magnesium improves hardenability, while copper is added to increase low-temperature strength (Ref 15).

X-ray diffraction (XRD) was carried out on A380M aluminum alloy employing a high-speed Bruker D8 Advance XRD system using Cu-Kα radiation having a wave length of 1.54 Å, tube voltage of 40 kV, and tube current of 40 mA (Fig. 1). Al and Si peaks were matched to those in the Powder Diffraction Files and identified as having FCC crystal structure. The XRD pattern for the A380M is shown in Fig. 2.

Mechanical properties of A380M aluminum alloy was measured using a nanoindentation system (developed by CETR, Campbell, CA). The instrument uses a Berkovich diamond pyramid with an angle of 65.3° between the tip axis and the faces of the triangular pyramid. The displacement of the indentation and the load could be measured independently with a resolution of 0.03 nm and 0.1 μN, respectively. The advantage of nanoindentation is that very thin area of surface can be measured. Twelve measurements at 12 different places were produced on a given specimen using maximum load range from 50 to 400 mN to insure that any irregularities in the surface cannot affect the hardness value. The total penetration depth consists of a plastic component and an elastic recovery component which occurs during the unloading. Maximum indentation depth (h_{max}) can be expressed as

$$h_{max} = h_c + \left[\frac{(\pi - 2)}{\pi}\right]\left(\frac{2P_{max}}{dp/dh}\right), \quad \text{(Eq 1)}$$

where p and h are load and indentation depth, respectively. h_{max}, P_{max}, and slope at maximum load dp/dh are determined from the load versus displacement profile. Hardness (H) at

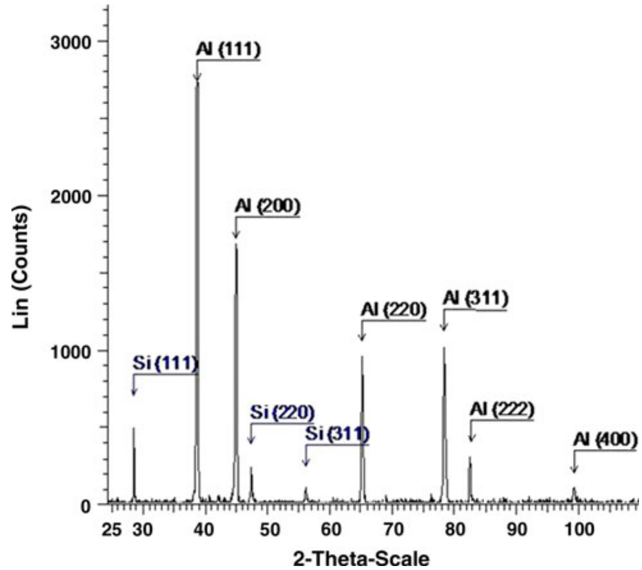

Fig. 2 XRD patterns of A380M

the maximum applied load was calculated using Oliver and Pharr method (Ref 16). The relationship between H and the maximum applied load (P_{max}) is as follows:

$$H = \frac{P_{max}}{A}, \quad \text{(Eq 2)}$$

where A is the area of contact, and for Berkovich indenter

$$A = 24.5h_c^2, \quad \text{(Eq 3)}$$

where h_c is the contact depth. The elastic modulus can be expressed as

$$E^* = \frac{1}{2}\frac{dp}{dh}\frac{\sqrt{\pi}}{\sqrt{A}}, \quad \text{(Eq 4)}$$

where

$$\frac{1}{E^*} = \frac{1 - \nu_1^2}{E_1} + \frac{1 - \nu_2^2}{E_2}. \quad \text{(Eq 5)}$$

Here, E_2 and ν_2 are elastic modulus and Poisson's ratio of the test material, respectively, and E_1 and ν_1 are the same parameters for Berkovich indenter. In the current analysis, E_1 and ν_1 were taken as 1141 GPa and 0.07, respectively. Force-displacement (penetration depth of indenter) curve shows the loading/unloading cycles of the nano-indentation test (Fig. 3). The calculated hardness and Young's modulus of A380M aluminum alloy are 1 and 50 GPa, respectively.

Dry reciprocating wear tests were performed using a Universal Micro-Tribometer (UMT) (CETR, Campbell, CA). This test method utilizes a ball upper specimen that slides against a flat lower specimen in a linear, back and forth, sliding motion having a stroke length of 5.03 mm. All tests were conducted at room temperature and at a relative humidity of 40 to 55%. The load is applied downward through the ball specimen against the flat specimen mounted on a reciprocating drive. The tester allows for monitoring the dynamic normal load, friction force, and depth of the wear track during the test. Figure 4 depicts an image of the wear chamber and the sliding ball of the UMT tribometer. The specimens were securely fastened inside the wear chamber.

A 6.3 mm diameter bearing steel (AISI 52100) ball having a hardness of HRA 83 was used as a counter-face material. The ball was mounted inside a ball holder which was attached directly to a suspension system, which, in turn, is attached to a load sensor that controls and records forces during the test. The instantaneous values of calibrated normal load (F_Z), tangential load (F_X), and depth of wear track (Z) were measured and continuously recorded, using a data acquisition system. The data automatically calculates the variation of the coefficient of friction, COF ($\mu = F_X/F_Z$) with time. The weight of the specimen was measured before and after each wear test to determine individual weight loss at selected time intervals.

Four different loads (6, 10, 15, and 20 N) were employed; each tested at four different frequencies (4, 10, 15, and 20 Hz) and at five different time intervals (10, 30, 45, 60, and 90 min).

The wear volume (V) was calculated according to the ASTM standard G133 (Ref 17) as follows:

$$V = \left(\frac{\pi h}{6}\right)\left[\frac{3D^2}{4} + h^{*2}\right], \quad \text{(Eq 6)}$$

where h^* is the depth of wear track (mm) and D is the effective diameter (mm). Assuming a spherical wear volume, the effective diameter, D, can be calculated from h using the following equation:

$$h^* = R - \left[R^2 - \left(\frac{D^2}{4}\right)\right]^2, \quad \text{(Eq 7)}$$

where R is the ball radius (mm).

After wear tests, worn surfaces and wear debris were examined using a Hitachi S-4700 scanning electron microscope to determine possible wear mechanism operating under different test conditions.

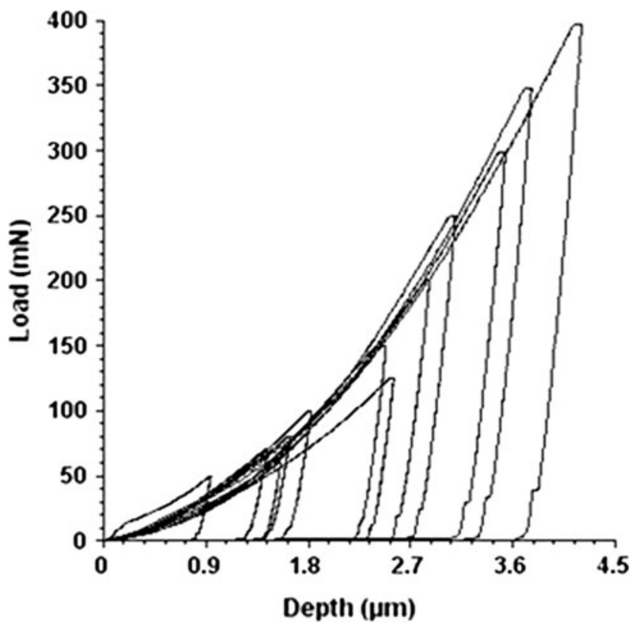

Fig. 3 Load vs. indentation depth profile

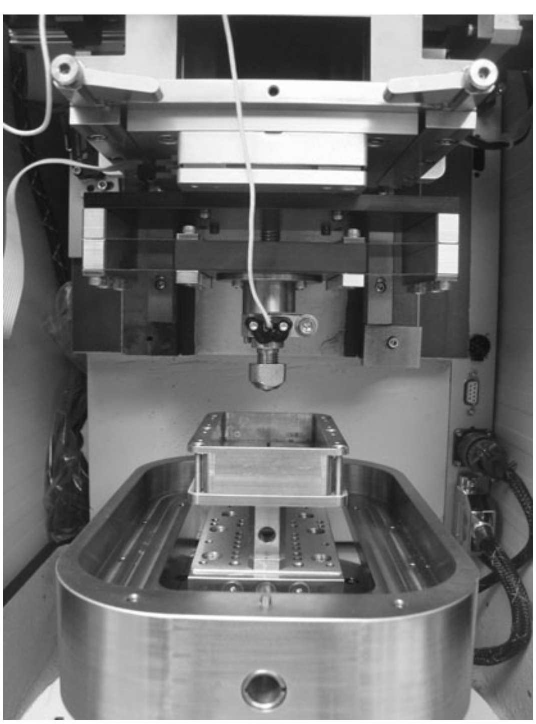

Fig. 4 Ball-on-flat reciprocating wear tester

3. Results and Discussion

The calculated cumulative weight loss versus sliding distance curves for four different loading conditions—6, 10, 15 and 20 N—at 4 Hz is shown in Fig. 5. They reveal a linear increase in weight loss with sliding distance for all loading conditions. Furthermore, the weight loss increases with load at any given sliding distance. This is because, with increase of the load, higher stress is induced in the subsurface region, which leads to subsurface nucleation of cracks with repeated loading. On the other hand, the amount of weight loss increases with increase in sliding distance as expected. The absence of any transitions indicates that the same wear mechanism is operative throughout the entire tests.

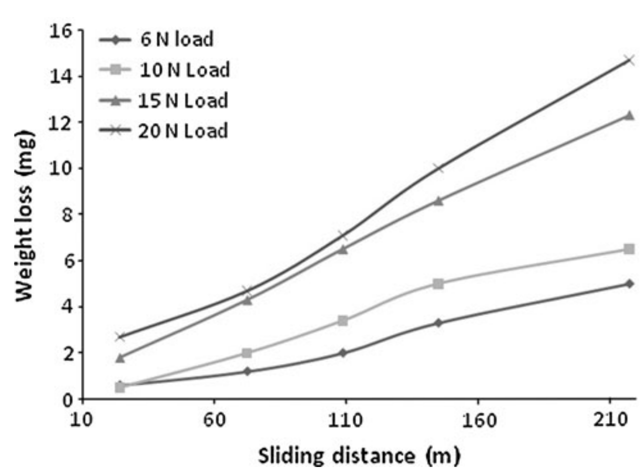

Fig. 5 The dependence of cumulative weight loss on load and sliding distance at 4 Hz

Wear rates, calculated as the slopes of the weight loss versus sliding distance curves under all conditions, are plotted as functions of applied loads and frequencies. Figure 6(a) reveals that the wear rate increases somewhat linearly with load; this has also been observed by others (Ref 18-20). On the other hand, Fig. 6(b) shows two regions in the wear rate versus frequency curves. Region 1 shows a rapid decrease in wear rate with increasing frequency up to 10 Hz followed by a second region at which the effect of the applied frequency on wear rate seems to be negligible. It is speculated that the initial drop in wear rate with increase in frequency is due to strain hardening. At high frequency, however, wear rate reaches a steady-state condition as the strain hardening effect, as a result of the high strain rate at high applied frequency, is offset by thermal softening due to frictional heating. The competition between strain hardening and thermal softening as the reciprocating frequency increases has been previously reported (Ref 21). Alwahdi et al. reported that wear rate decreases with increasing strain hardening ratio (Ref 22).

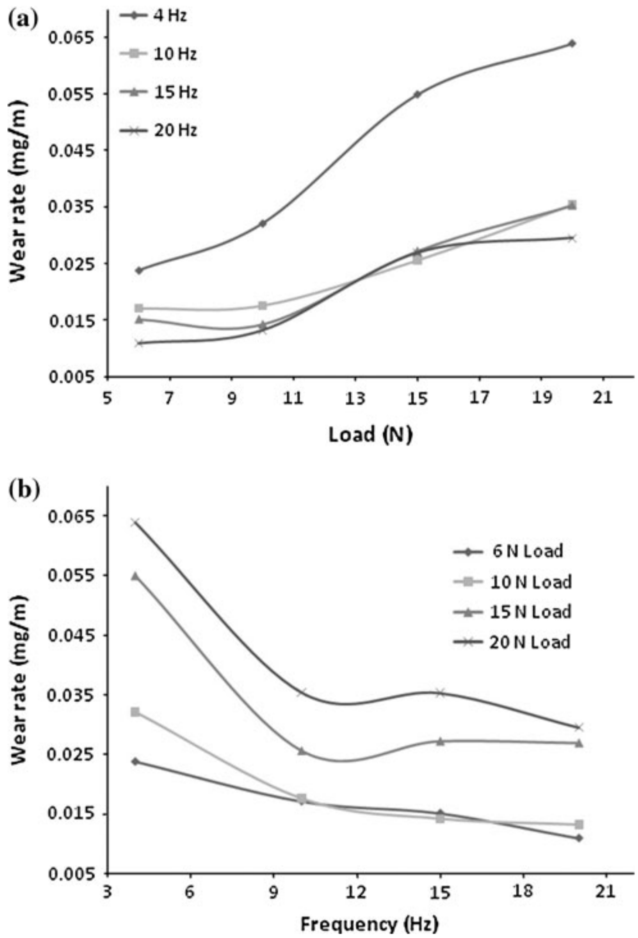

Fig. 6 (a) Wear rate vs. load at different frequencies. (b) Wear rate vs. frequency for different loads

Coefficient of friction (COF) and wear track depth (Z) versus time curves for A380M at 4 Hz and 10 N are shown in Fig. 7, as representative examples of the data collected during wear tests. The COF curves for all tests show similar overall shapes. A typical behavior of COF during a test is that it initially increases quickly to a high value (break-in period) followed by decrease in steady-state value. The cumulative wear track depth (Z) versus time exhibited a reasonably linear rise with time after a short break-in period. The coefficient of friction decreases with the increase in frequency (Fig. 8) for A380M aluminum alloy. The magnitude of plastic strain gradient and depth of highly deformed zone depend on COF (Ref 23). It is suspected that at low frequency, longer time is available for the formation and growth of junction asperity contact regions, which increases the force required to shear off the junction to maintain relative motion. Dwivedi (Ref 24) reported similar findings for cast hypereutectic aluminum silicon alloys. Furthermore, it was observed that COF slightly increases with the applied load. Sadik in his experiment showed that coefficient of friction remains constant with time (Ref 25).

The measured wear track depth Z (defined as h^* in Eq 6 and 7) is converted to volume loss using Eq 6 and 7. The volume loss for different loading conditions is plotted with respect to sliding distance in Fig. 9. Wear behavior observed using depth

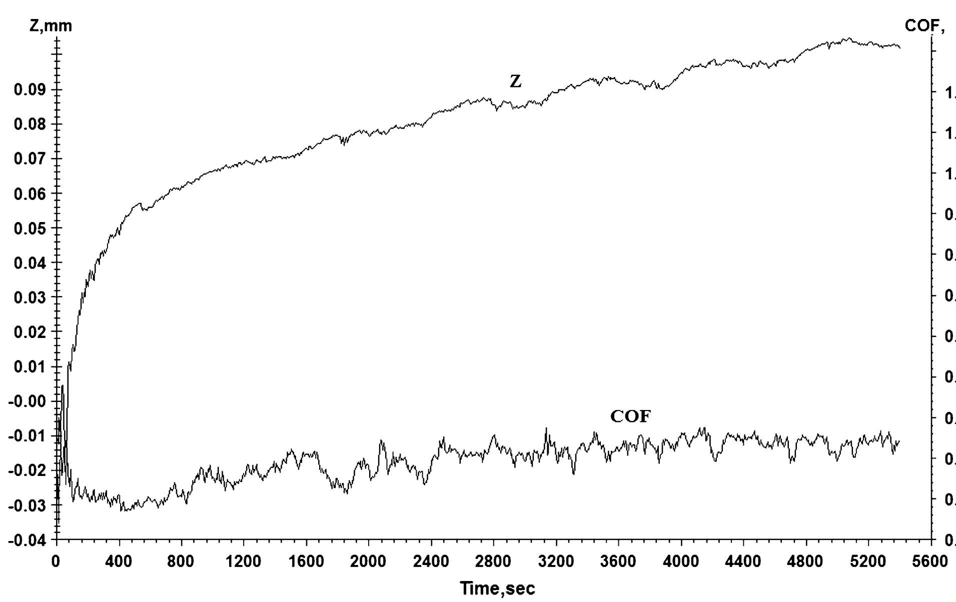

Fig. 7 Coefficient of friction (COF) and wear track depth (Z) vs. time at a frequency of 4 Hz and 10 N normal load

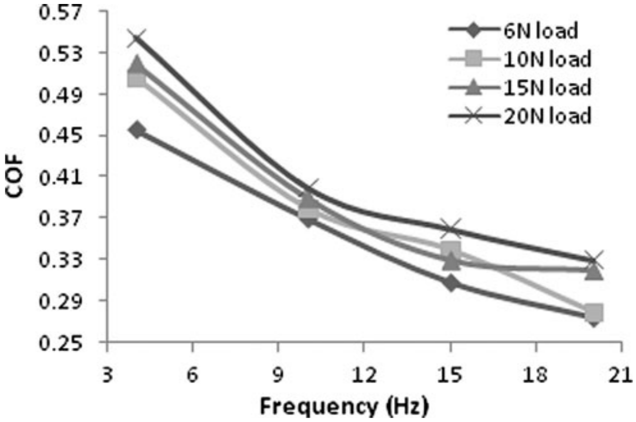

Fig. 8 Coefficient of friction vs. frequency at different load

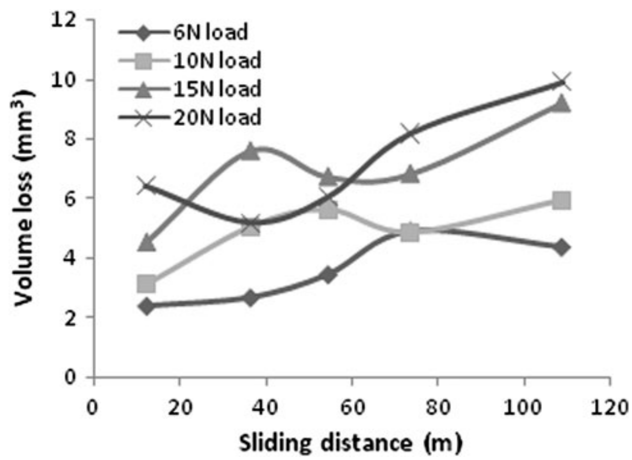

Fig. 9 Volume loss vs. sliding distance at a frequency of 4 Hz

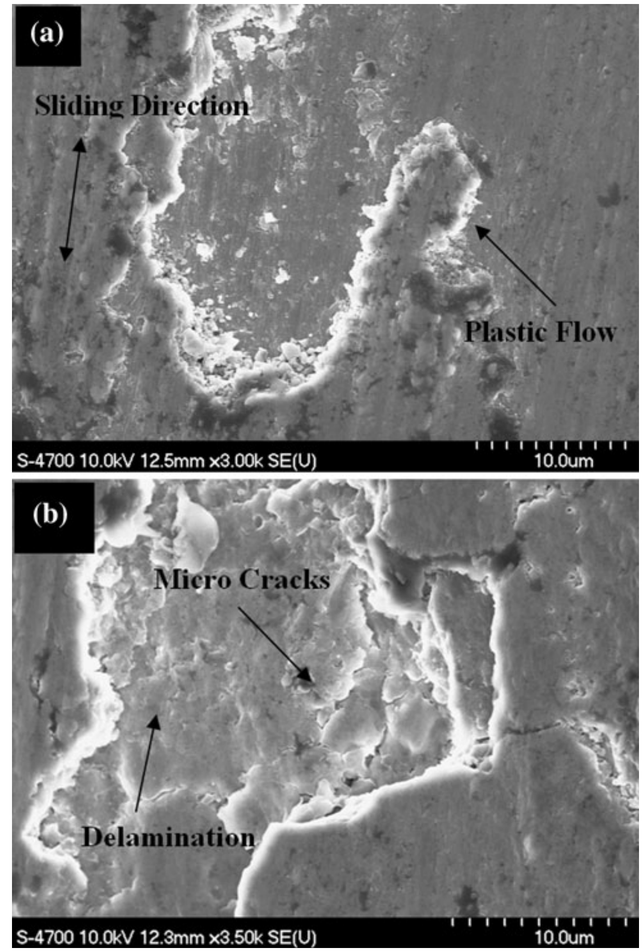

Fig. 10 Wear track of A380M aluminum alloy at 20 Hz and 20 N load: (a) Plastic flow. (b) Delamination

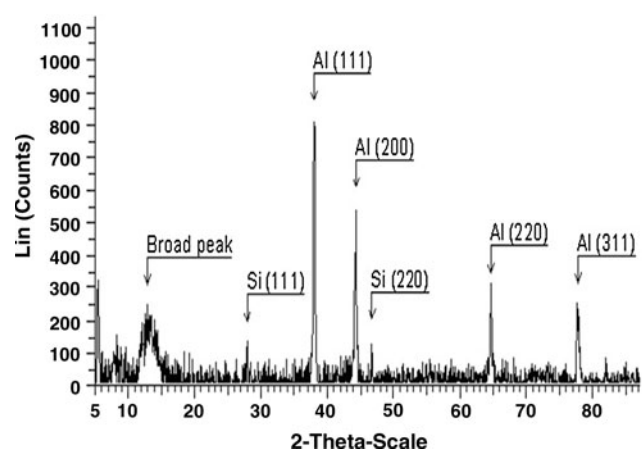

Fig. 11 XRD pattern of wear debris

of wear track reveals fluctuations as compared to weight loss. The volume losses are calculated based on the depth of the wear track (*Z*). Due to the irregularities and wear debris in the wear track, localized fluctuation in the *Z* values can occur. Therefore, it is concluded that wear rates can be more accurately measured using weight loss experiments. However, general trend over a large sliding distance is increasing.

Two wear mechanisms have been identified as dominant mechanisms during dry sliding wear of A380M aluminum alloy, namely, abrasion and delamination. Figure 10 shows the wear tracks of A380M aluminum alloy at 20 Hz frequency and 20 N load. The wear tracks of the samples were characterized by heavy plastic deformation and damage in the form of plastic flow extending parallel to the sliding direction (Fig. 10a). Moreover, at high normal load, a high shear stress is induced in the subsurface region and with repeated cycling it eventually leads to subsurface nucleation and propagation of cracks. When these subsurface cracks reach a critical length, they become unstable and propagate to the surface, generating plate-like wear debris leaving behind a large pit on the worn surface (Fig. 10b). This type of wear is known as delamination wear.

A notable feature of an XRD pattern of wear debris is the presence of a diffuse but distinct peak at Bragg's angle (2θ) between 10° and 15° (Fig. 11). This suggests either the presence of an amorphous phase, such as Al_2O_3, or the formation of a nanocrystalline phase due to the heavy deformation during wear. SEM examination of wear debris of A380M aluminum alloy at 20 Hz and 20 N reveals two types of wear particles (Fig. 12). The first type has an equiaxed irregular morphology (<5 μm in size), and the second type has a plate like morphology (40 μm wide and 7 μm thick). The fine

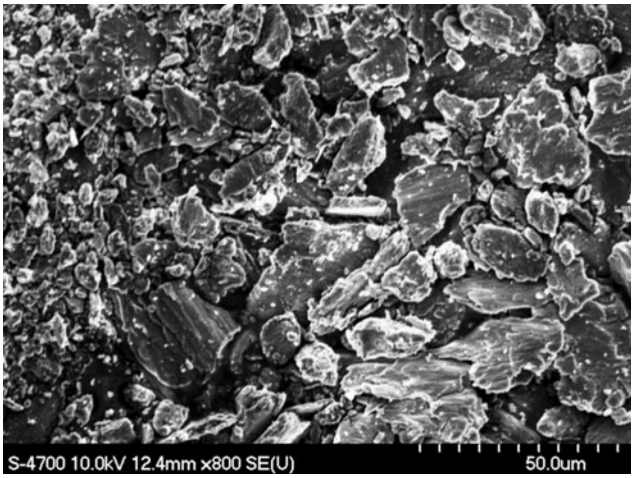

Fig. 12 Wear debris of A380M aluminum alloy at 20 Hz and 20 N

wear debris is believed to be a result of abrasive wear, and the coarse plate-like particles are a result of delamination wear.

4. Conclusion

Wear of A380M aluminum alloy was investigated under reciprocating contacts against a steel ball. The experimental study was carried out under different normal loads, frequencies, and durations. It was found that the wear of A380M aluminum alloy increased gradually with increasing load. At low load, wear debris in the contact region caused surface deformation and abrasion by three-body abrasion mechanism. At high load, however, delamination wear seemed to be the dominant wear mechanism. As a result of high subsurface shear stress, cracks form and propagate to the surface, leading to the formation of plate-like wear debris. It was also observed that increasing frequency resulted in decreasing wear rate due to strain hardening effect resulting from high strain rate. At high reciprocating frequency, frictional heat generated at the contact surface resulted in thermal softening of the aluminum surface layer, thus offsetting strain hardening effects and ultimately leading to a plateau in wear rate. The relationship between the coefficient of friction and frequency suggests that at lower frequency longer time is available for the formation and growth of asperity junctions which gives rise to higher coefficient of friction.

Acknowledgments

The authors would like to thank Auto-21 for financial support and Magna power train for providing A380M aluminum alloy.

References

1. N. Saka, A.M. Eleiche, and N.P. Suh, Wear of Metals at High Sliding Speeds, *Wear*, 1977, **44**(1), p 109–125
2. Y. Liu, R. Asthana, and P. Rohatgi, A Map for Wear Mechanisms in Aluminum Alloys, *J. Mater. Sci.*, 1991, **26**, p 99–102
3. F.F. Ling and E. Saibel, Thermal Aspects of Galling of Dry Metallic Surfaces in Sliding Contact, *Wear*, 1957, **1**(2), p 80–91
4. C. Subramanian, Effects of Sliding Speed on the Unlubricated Wear Behaviour of Al-12.3wt.%Si Alloy, *Wear*, 1991, **151**(1), p 97–110
5. K. Mohammed Jasim and E.S. Dwarakadasa, Effect of Sliding Speed on Adhesive Wear of Binary Al-Si Alloys, *J. Mater. Sci. Lett.*, 1993, **12**, p 650–653
6. S.K. Biswas and B.N. Parmila Bai, Dry Wear of Al-Graphite Particle Composites, *Wear*, 1981, **68**(3), p 347–358
7. R. Shivanath, P.K. Sengupta, and T.S. Eyre, Wear of Aluminum–Silicon Alloys, *Br. Foundrymen*, 1977, **70**(12), p 349
8. R.S. Yassen and E.S. Dwarakadasa, Wear of Aluminium Under Dry Sliding Conditions, *Wear*, 1983, **84**(3), p 375–379
9. S. Wilson and A.T. Alpas, Thermal Effects on Mild Wear Transitions in Dry Sliding of an Aluminum Alloy, *Wear*, 1999, **225–229**(1), p 440–449
10. J. Zhang and A.T. Alpas, Transition Between Mild and Severe Wear in Aluminum Alloys, *Acta Metall. Mater.*, 1997, **45**, p 513–528
11. A.D. Sarkar and J. Clacke, Friction and Wear of Aluminium-Silicon Alloys, *Wear*, 1980, **61**(1), p 157–167
12. K. Tingler, "A Developmental Study in Tensile Properties of Plaster cast A356 Aluminum Alloy at Room and Elevated Temperature", Oklahoma State University Stillwater, OK, 2008, UMI no 1461826, p 21
13. A.D. Sarkar and J. Clarke, Wear Characteristics of As-Cast Binary Aluminium-Silicon Alloys, *Wear*, 1979, **54**(1), p 7–16
14. J.R. Gomes, A. Ramalho, M.C. Gaspar, and S.F. Carvalho, Reciprocating Wear Tests of Al–Si/SiCp Composites: A Study of the Effect of Stroke Length, *Wear*, 2005, **259**(1–6), p 545–552
15. Y. Ma, "Integrated Study of the Influence of Casting and Heat Treatment Parameters on Microstructures of Multiphase Multi-Component Aluminum Alloys", Dissertation, University of Connecticut, 2008, p 10
16. W.C. Oliver and G.M. Pharr, Improved Technique for Determining Hardness and Elastic Modulus Using Load and Displacement Sensing Indentation Experiments, *J. Mater. Res.*, 1992, **74**, p 1564–1580
17. "Standard Test Method for Linearly Reciprocating Ball-on-Flat Sliding Wear," G 133 – 05, Annual Book of ASTM Standards
18. M. Hiratsuka, Role of Wear Particles in Severe-Mild Wear Transition, *Wear*, 2005, **259**(1–6), p 467–476
19. A.T. Alpas and J. Zhang, Wear Rate Transition in Cast Aluminum-Silicon Alloys Reinforced with SiC Particles, *Scripta Metall.*, 1992, **26**, p 505–509
20. A.A. Hamid, P.K. Ghosh, S.C. Jain, and S. Ray, The Influence of Porosity and Particles Content on Dry Sliding Wear of Cast In Situ Al(Ti)-Al2O3(TiO2) Composite, *Wear*, 2008, **265**, p 14–26
21. W. Hirst and J.K. Lancaster, The Influence of Speed on Metallic Wear, *Proc. Roy. Soc.*, 1960, **A259**, p 229
22. F. Alwahdi, F.J. Franklin, and A. Kapoor, The Effect of Partial Slip on the Wear Rate of Rails, *Wear*, 2005, **258**, p 1031–1037
23. P.L. Menezes, Kishore, and S.V. Kailas, Role of Surface Texture of Harder Surface on Subsurface Deformation, *Wear*, 2009, **266**, p 103–109
24. D.K. Dwivedi, Wear Behavior of Cast Hypereutectic Aluminum Silicon Alloys, *Mater. Des.*, 2006, **27**, p 610–616
25. B. Sadik, Investigation of Tribological and Mechanical Properties of Metal Bearing, *Bull. Mater. Sci.*, 2009, **32**(4), p 451–457